npj | Quantum Information

www.nature.com/npjqi

ARTICLE OPEN

Characterizing the multipartite continuous-variable entanglement structure from squeezing coefficients and the Fisher information

Zhongzhong Qin[1,2], Manuel Gessner[3], Zhihong Ren[1,2,4], Xiaowei Deng[1,2], Dongmei Han[1,2], Weidong Li[1,2,4], Xiaolong Su[1,2], Augusto Smerzi[3,5] and Kunchi Peng[1,2]

Understanding the distribution of quantum entanglement over many parties is a fundamental challenge of quantum physics and is of practical relevance for several applications in the field of quantum information. The Fisher information is widely used in quantum metrology since it is related to the quantum gain in metrology measurements. Here, we use methods from quantum metrology to microscopically characterize the entanglement structure of multimode continuous-variable states in all possible multi-partitions and in all reduced distributions. From experimentally measured covariance matrices of Gaussian states with 2, 3, and 4 photonic modes with controllable losses, we extract the metrological sensitivity as well as an upper separability bound for each partition. An entanglement witness is constructed by comparing the two quantities. Our analysis demonstrates the usefulness of these methods for continuous-variable systems and provides a detailed geometric understanding of the robustness of cluster-state entanglement under photon losses.

npj Quantum Information (2019)5:3 ; https://doi.org/10.1038/s41534-018-0119-6

INTRODUCTION

Entanglement plays a central role in quantum information science,[1–3] in particular for quantum computation[4–6] and quantum metrology.[7] An efficient analysis of the quantum resources for such applications requires a detailed understanding of the correlation structure of multipartite quantum states and the development of experimentally feasible methods for their experimental characterization.[8]

Entanglement of continuous-variable (CV) systems has been studied intensively over the past years.[2,3] The most common method for the analysis of bi-partitions is the positive partial transposition (PPT) criterion, which is highly efficient and easy to implement for Gaussian states.[9,10] Providing a microscopic picture of the entanglement structure in terms of all possible combinations of subsystems, i.e., multi-partitions, is a considerably more difficult task.[11] Multipartite CV entanglement criteria for specific partitions can be derived from uncertainty relations[12] or by systematic construction of entanglement witnesses.[13] While criteria of this kind are experimentally convenient in many cases,[14–17] they require the additional effort of determining the separability bound as a function of the observables at hand, which can be a complicated problem in general. Moreover, abstract entanglement witnesses usually provide little intuition about the physical significance and origin of the entanglement.

The Fisher information relates the multipartite entanglement between the subsystems to the sensitivity for quantum parameter estimation.[18] This approach has proven to be extremely successful with discrete-variable systems, especially for spin systems of cold atoms.[19] The Fisher information can furthermore be efficiently approximated for Gaussian spin states by means of experimentally convenient spin squeezing coefficients.[20,21] Using these methods, multipartite entanglement of large numbers of particles has been demonstrated by collective measurements.[19,22–24]

An extension of the theoretical framework to CV systems has been achieved recently by combining the quantum Fisher information with local variances[18] and the development of a bosonic multi-mode squeezing coefficient.[25] The squeezing coefficient is based on a second-order approximation of the quantum Fisher information and represents an easily accessible entanglement criterion. A microscopic understanding of the inseparability properties in all possible partitions of the system is provided by the information from local measurements on the subsystems. Local observables are routinely measured in CV systems, such as photonic cluster states.[16,17,26] The separability bounds for the metrological sensitivity are directly obtained from the local data and need not be determined theoretically. Entanglement criteria based on the quantum Fisher information further provide a geometric interpretation in phase space.

Here, we analyze experimentally generated CV multi-mode entangled states of two, three, and four photonic modes using the recently developed bosonic squeezing coefficients and the CV quantum Fisher information. Our complete microscopic mode-by-mode study encompasses all possible multi-partitions of the systems as well as the reduced distributions obtained by tracing over certain modes. A controllable loss channel on one of the modes is used to study the effect of losses on the multipartite

[1]State Key Laboratory of Quantum Optics and Quantum Optics Devices, Institute of Opto-Electronics, Shanxi University, Taiyuan 030006, China; [2]Collaborative Innovation Center of Extreme Optics, Shanxi University, Taiyuan 030006 Shanxi, China; [3]QSTAR, INO-CNR and LENS, Largo Enrico Fermi 2, I-50125 Firenze, Italy; [4]Institute of Theoretical Physics and Department of Physics, Shanxi University, Taiyuan 030006, China and [5]Institute of Laser Spectroscopy, Shanxi University, Taiyuan 030006, China
Correspondence: Weidong Li (wdli@sxu.edu.cn) or Xiaolong Su (suxl@sxu.edu.cn)
These authors contributed equally: Zhongzhong Qin, Manuel Gessner, Zhihong Ren.

Received: 12 August 2018 Accepted: 9 December 2018
Published online: 04 January 2019

entanglement structure. Our analysis is based on experimentally extracted covariance matrices and demonstrates the applicability of entanglement criteria based on the Fisher information to CV systems and cluster states. Sudden transitions as a function of loss and noise-independent partitions are explained intuitively by the geometric interpretation of our entanglement criteria in phase space. Finally, we show that the criteria are not equivalent to the Gaussian PPT criterion, which can only be applied to bi-partitions.

RESULTS

CV entanglement criteria from squeezing coefficients and Fisher information

We consider an N-mode CV system with a vector of phase-space operators $\hat{\mathbf{r}} = (\hat{r}_1, \ldots, \hat{r}_{2N}) = (\hat{x}_1, \hat{p}_1, \ldots, \hat{x}_N, \hat{p}_N)$. Any real vector $\mathbf{g} = (g_1, \ldots, g_{2N})$ defines a multi-mode quadrature $\hat{q}(\mathbf{g}) = \mathbf{g} \cdot \hat{\mathbf{r}}$, which generates displacements of the form $\hat{D}(\theta) = \exp(-i\hat{q}(\mathbf{g})\theta)$. The sensitivity of a Gaussian quantum state $\hat{\rho}$ under such displacements is determined by the quantum Fisher information[27–29]

$$F_Q[\hat{\rho}, \hat{q}(\mathbf{g})] = \mathbf{g}^T \mathbf{\Omega}^T \mathbf{\Gamma}_{\hat{\rho}}^{-1} \Omega \mathbf{g}, \tag{1}$$

where $\mathbf{\Omega} = \oplus_{i=1}^{N} \begin{pmatrix} 0 & 1 \\ -1 & 0 \end{pmatrix}$ is the symplectic form and $\mathbf{\Gamma}_{\hat{\rho}}^{-1}$ is the inverse of the covariance matrix with elements $(\mathbf{\Gamma}_{\hat{\rho}})_{ij} = \frac{1}{2}\langle \hat{r}_i \hat{r}_j + \hat{r}_j \hat{r}_i \rangle_{\hat{\rho}} - \langle \hat{r}_i \rangle_{\hat{\rho}} \langle \hat{r}_j \rangle_{\hat{\rho}}$. By means of the quantum Cramér–Rao inequality, the quantum Fisher information directly determines the precision bound for a quantum parameter estimation of θ. It was shown in ref. [18] that an upper limit for the sensitivity of mode-separable states is given in terms of the single-mode variances of the same state:

$$F_Q[\hat{\rho}_{\text{sep}}, \hat{q}(\mathbf{g})] \leq 4\mathbf{g}^T \mathbf{\Gamma}_{\Pi(\hat{\rho}_{\text{sep}})} \mathbf{g}, \tag{2}$$

where $\mathbf{\Gamma}_{\Pi(\hat{\rho}_{\text{sep}})}$ is the covariance matrix after all elements except the central 2×2 blocks have been set to zero, effectively removing all mode correlations. This corresponds to the covariance matrix of the product state of the reduced density matrices $\Pi(\hat{\rho}) = \otimes_{i=1}^{N} \hat{\rho}_i$. Any violation of inequality (2) indicates the presence of entanglement between the modes. To identify the contribution of specific subsystems in a multipartite system, this criterion can be generalized for a microscopic analysis of the entanglement structure.[25] A witness for entanglement in a specific partition of the full system into subsystems $\Lambda = \mathcal{A}_1 | \ldots | \mathcal{A}_M$, where $\mathcal{A}_l$ describes an ensemble of modes, is obtained from Eq. (2) by replacing the fully separable product state $\Pi(\hat{\rho})$ on the right-hand side by a product state on the partition $\mathcal{A}_1 | \ldots | \mathcal{A}_M$. More precisely, any $\mathcal{A}_1 | \ldots | \mathcal{A}_M$-separable quantum state, i.e., any state that can be written as $\hat{\rho}_\Lambda = \sum_\gamma p_\gamma \hat{\rho}_{\mathcal{A}_1}^{(\gamma)} \otimes \ldots \otimes \hat{\rho}_{\mathcal{A}_M}^{(\gamma)}$, where p_γ is a probability distribution, must satisfy[25]

$$F_Q[\hat{\rho}_\Lambda, \hat{q}(\mathbf{g})] \leq 4\mathbf{g}^T \mathbf{\Gamma}_{\Pi_\Lambda(\hat{\rho}_\Lambda)} \mathbf{g}, \tag{3}$$

where $\Pi_\Lambda(\hat{\rho}_\Lambda) = \otimes_{l=1}^{M} \hat{\rho}_{\mathcal{A}_l}$ and $\hat{\rho}_{\mathcal{A}_l}$ is the reduced density matrix of $\hat{\rho}_\Lambda$ on $\mathcal{A}_l$. The covariance matrix $\mathbf{\Gamma}_{\Pi_\Lambda(\hat{\rho}_\Lambda)}$ can be easily obtained from $\mathbf{\Gamma}_{\hat{\rho}_\Lambda}$ by setting only those off-diagonal blocks to zero which describe correlations between different subsystems $\mathcal{A}_l$. The fully separable case, Eq. (2), is recovered if each $\mathcal{A}_l$ contains exactly one mode.

By combining the separability criterion (3) with the expression for the quantum Fisher information of Gaussian states (1), we find the following condition for the covariance matrix of $\mathcal{A}_1 | \ldots | \mathcal{A}_M$-separable states:

$$\mathbf{\Gamma}_{\hat{\rho}}^{-1} - 4\mathbf{\Omega}^T \mathbf{\Gamma}_{\Pi_\Lambda(\hat{\rho})} \mathbf{\Omega} \leq 0, \tag{4}$$

where we have used that both expressions (1) and (3) are valid for arbitrary $\mathbf{g}$ and then multiplied the equation with $\mathbf{\Omega}$ from both sides using $\mathbf{\Omega}^T \mathbf{\Omega} = \mathbb{1}_{2N}$ and $\mathbf{\Omega}^T = -\mathbf{\Omega}$. Inequality (4) expresses that the matrix on the left-hand side must be negative semidefinite. Hence, if we find a single positive eigenvalue, entanglement in the considered partition is revealed. Thus, it suffices to check whether the maximal eigenvalue $\lambda_{\max}$ is positive. The corresponding eigenvector $\mathbf{e}_{\max}$ further identifies a $2N$-dimensional "direction" in phase space such that the sensitivity under displacements generated by $\hat{q}(\mathbf{e}_{\max})$ maximally violates Eq. (3).

A lower bound on the quantum Fisher information of arbitrary states can be found from elements of the covariance matrix using[25]

$$F_Q[\hat{\rho}, \hat{q}(\mathbf{g})] \geq \frac{(\mathbf{h}^T \mathbf{\Omega} \mathbf{g})^2}{\mathbf{h}^T \mathbf{\Gamma}_{\hat{\rho}} \mathbf{h}}, \tag{5}$$

which holds for arbitrary $\mathbf{g}$, $\mathbf{h}$. Choosing $\mathbf{h} = \mathbf{\Omega}\mathbf{g}$ with $|\mathbf{g}|^2 = 1$ leads with (3) to the separability condition[25]

$$\xi_\Lambda^{-2}(\hat{\rho}_{\text{sep}}) \leq 1, \tag{6}$$

where

$$\xi_\Lambda^2(\hat{\rho}) := \min_{\mathbf{g}} 4(\mathbf{g}^T \mathbf{\Omega}^T \mathbf{\Gamma}_{\Pi_\Lambda(\hat{\rho})} \mathbf{\Omega} \mathbf{g})(\mathbf{g}^T \mathbf{\Gamma}_{\hat{\rho}} \mathbf{g}), \tag{7}$$

is the bosonic multi-mode squeezing coefficient for the partition Λ. Here, the minimizing $\mathbf{g}$ can be interpreted as a direction in phase space that identifies a multi-mode quadrature $\hat{q}(\mathbf{g})$ with a squeezed variance which can be traced back to mode entanglement.[25]

Experimental setup

In the following, we analyze experimentally generated N-mode Gaussian states with $N = 2, 3, 4$, subject to asymmetric loss using the two entanglement criteria defined by the quantum Fisher information, Eq. (4), and the multi-mode squeezing coefficient, Eq. (6). The graph representations of the three classes of Gaussian multi-mode entangled states considered here are shown in Fig. 1. They are often referred to as CV two-mode Gaussian entangled state ($N = 2$, Fig. 1a), three-mode CV Greenberger–Horne–Zeilinger (GHZ) state ($N = 3$, Fig. 1b), and four-mode square Gaussian cluster state ($N = 4$, Fig. 1c). The experimental generation of the states is described in detail in the Methods section and refs. [30,31] In all cases, the CV entangled states are generated by nondegenerate optical parametric amplifiers (NOPAs) with -3 dB squeezing at the sideband frequency of 3 MHz. The two-mode Gaussian entangled state is prepared directly by a NOPA. The three-mode GHZ state is obtained by combining a phase-squeezed and two amplitude-squeezed states using two beam splitters with transmissivities of $T_1 = 1/3$ and $T_2 = 1/2$, respectively, as shown in Fig. 1d.[30] Similarly, the four-mode square Gaussian cluster state is prepared by coupling two phase-squeezed and two amplitude-squeezed states on a beam-splitter network consisting of three beam splitters with $T_3 = 1/5$ and $T_4 = T_5 = 1/2$, respectively, as shown in Fig. 1e.[31]

To study the robustness of multipartite entanglement under transmission losses, a lossy quantum channel for mode A is simulated using a half-wave plate (HWP) and a polarizing beam splitter (PBS). The output mode is given by $\hat{A}' = \sqrt{\eta}\hat{A} + \sqrt{1-\eta}\hat{v}$, where η and $\hat{v}$ represent the transmission efficiency of the quantum channel and the vacuum mode induced by loss into the quantum channel, respectively, as shown in Fig. 1f–h. Let us now turn to the characterization of CV entanglement based on the experimentally generated data.

Experimental results

Figure 2a shows the inverse squeezing coefficient (7) $\xi_{A|B}^{-2}$ for a CV two-mode Gaussian entangled state in a lossy channel (LC) for the only possible partition $A|B$ of the bipartite system. The coefficient

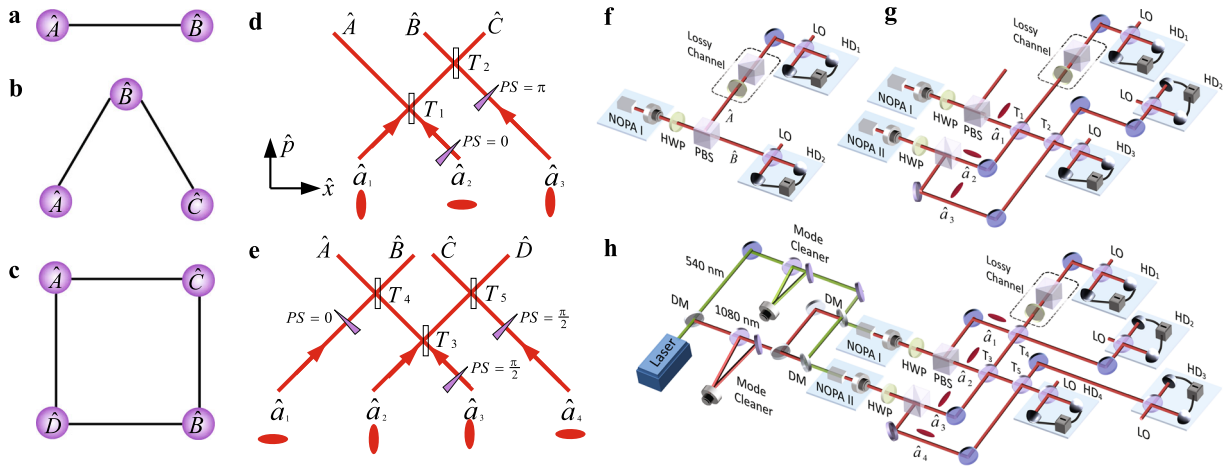

Fig. 1 Graph representation of multipartite CV entangled states and their preparation. **a** CV two-mode Gaussian entangled state. **b** Three-mode GHZ state. **c** Four-mode square Gaussian cluster state, respectively. **d**, **e** show the beam-splitter network used to generate the three-mode GHZ state and four-mode square Gaussian cluster state, respectively. The phase shift (PS) is realized by locking the relative phase of two light beams at the corresponding beam splitter. **f**–**h** show the schematics of preparation and measuring the two-mode Gaussian entangled state, three-mode GHZ state, and four-mode square Gaussian cluster state, respectively. PS phase shift, NOPA nondegenerate optical parametric amplifier, HWP half-wave plate, PBS polarizing beam splitter, LO local oscillator, HD_{1-4} homodyne detectors, DM dichroic mirror

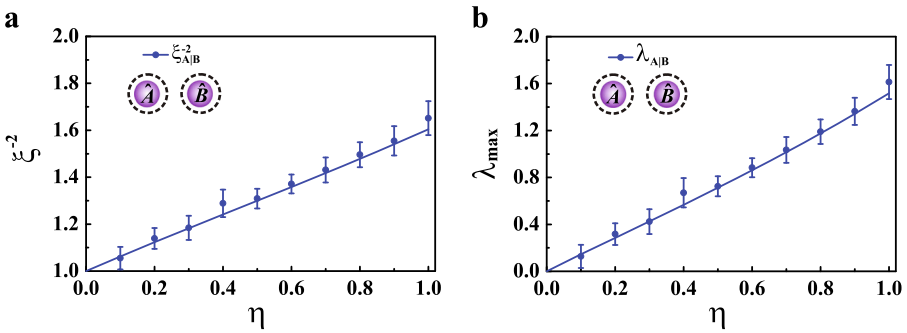

Fig. 2 Experimental results for the CV two-mode Gaussian entangled state in a lossy channel with transmission efficiency η. **a** Inverse multi-mode squeezing coefficients (7). The plot shows the squeezing coefficient $\xi^{-2}_{A|B}$ obtained by numerically minimizing in Eq. (7), using the experimentally measured covariance matrices (blue dots) and the theoretical prediction based on the state preparation schemes described in Fig. 1 (blue line). Values above one violate (6) and indicate entanglement. **b** Gaussian quantum Fisher information entanglement criterion, expressed by the maximum eigenvalue of the matrix on the left-hand side (l.h.s.) of Eq. (4). Positive values violate the separability condition (4). The error bars represent one standard deviation and are obtained from the statistics of the measured data

$\xi^{-2}_{A|B}$ decreases as the transmission efficiency η decreases but it always violates the separability condition (6) unless $\eta = 0$, i.e., when mode A is completely lost. This confirms that CV two-mode Gaussian entanglement only decreases but never fully disappears due to particle losses, i.e., CV two-mode Gaussian entanglement is robust to loss.[32] We observe the same behavior for the criterion Eq. (4), which makes use of the Gaussian quantum Fisher information. Figure 2b shows the maximum eigenvalue $\lambda_{\max}$ of the matrix $\mathbf{\Gamma}^{-1}_{\hat{\rho}} - 4\mathbf{\Omega}^T\mathbf{\Gamma}_{\hat{\rho}_A\otimes\hat{\rho}_B}\mathbf{\Omega}$. According to Eq. (4), a positive value indicates entanglement. Both coefficients attain their two-fold degenerate maximal value for the phase space directions $\mathbf{g} = (\sin\phi, 0, \cos\phi, 0)$ and $\mathbf{g} = (0, -\sin\phi, 0, \cos\phi)$, where ϕ is a function of η (for $\eta = 1$ we have $\phi = \pi/4$ [25]). These directions indicate strong correlations in the momentum quadratures and anti-correlations in the position quadratures, allowing us to relate the entanglement to the squeezing of the collective variances $\Delta(\hat{x}_A\sin\phi + \hat{x}_B\cos\phi)^2$ and $\Delta(\hat{p}_A\sin\phi - \hat{p}_B\cos\phi)^2$. It should be noted that $\xi^{-2}_{A|B}$ and $\xi^{-2}_{B|A}$ ($\lambda_{A|B}$ and $\lambda_{B|A}$) are identical because the entanglement coefficients only depend on the partition and not on the order in which the subsystems are labeled.

The entanglement structure becomes more interesting for the three-mode GHZ state, exhibiting four non-trivial partitions of the system, as well as three reduced two-mode states. The squeezing coefficient (7), as well as the Gaussian Fisher information entanglement criterion (4), are plotted in Fig. 3 for all four partitions. Both show that at $\eta = 1$, the three bi-separable partitions $A|BC$, $B|AC$, and $C|AB$ are equivalent due to the symmetry of the state, but as η is decreased, the entanglement in the partition $A|BC$ is more strongly affected by the losses than that of the other two partitions. In the extreme case where mode A is fully lost ($\eta = 0$) there is still some residual entanglement between B and C.[33] In this case, all partitions are equivalent to the bi-partition $B|C$. The data shown in Fig. 3 confirms this: In both cases, the entanglement witness for all partitions coincide at $\eta = 0$, except $A|BC$ which, as expected, yields zero.

We further notice a discontinuity for the theoretical predictions of both witnesses regarding the fully separable partition $A|B|C$ as a function of η (blue lines in Fig. 3). This can be explained by analyzing the corresponding optimal phase space direction $\mathbf{g}$. In the presence of only moderate losses, the maximal correlations and squeezing are identified along the direction $\mathbf{g} = (0, c_1, 0, c_2, 0, c_2)$ with $c_1^2 + 2c_2^2 = 1$, i.e., the multi-mode quadrature $\hat{q}(\mathbf{g}) = c_1\hat{p}_A + c_2\hat{p}_B + c_2\hat{p}_C$ which involves all three modes. The squeezing along this phase-space direction diminishes with increasing losses. When the losses of mode A become dominant, the squeezing along the phase space direction $\mathbf{g} = (0, 0, 1, 0, -1, 0)/\sqrt{2}$, i.e., of

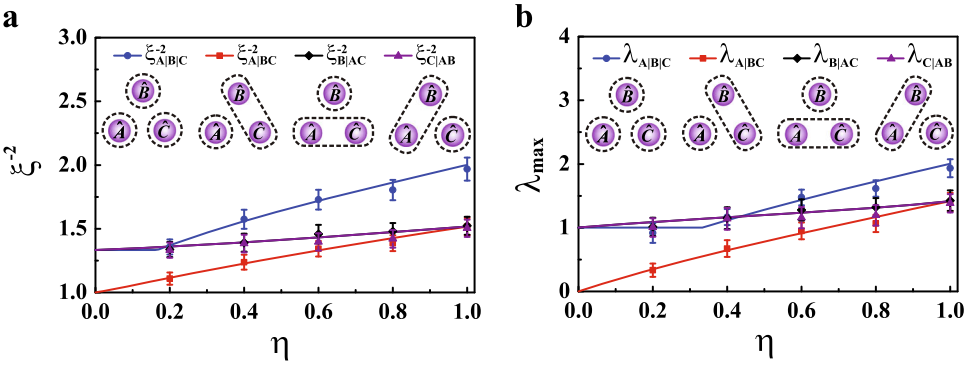

Fig. 3 Experimental results for the three-mode GHZ state in a lossy channel with transmission efficiency η. **a** Inverse multi-mode squeezing coefficients. **b** Gaussian Fisher information entanglement criterion. Shown are numerically optimized coefficients for the partitions $A|BC$ (blue circles), $A|BC$ (red squares), $B|AC$ (black diamonds), and $C|AB$ (purple triangles) from experimentally obtained covariance matrices and the curves represent the theoretical prediction

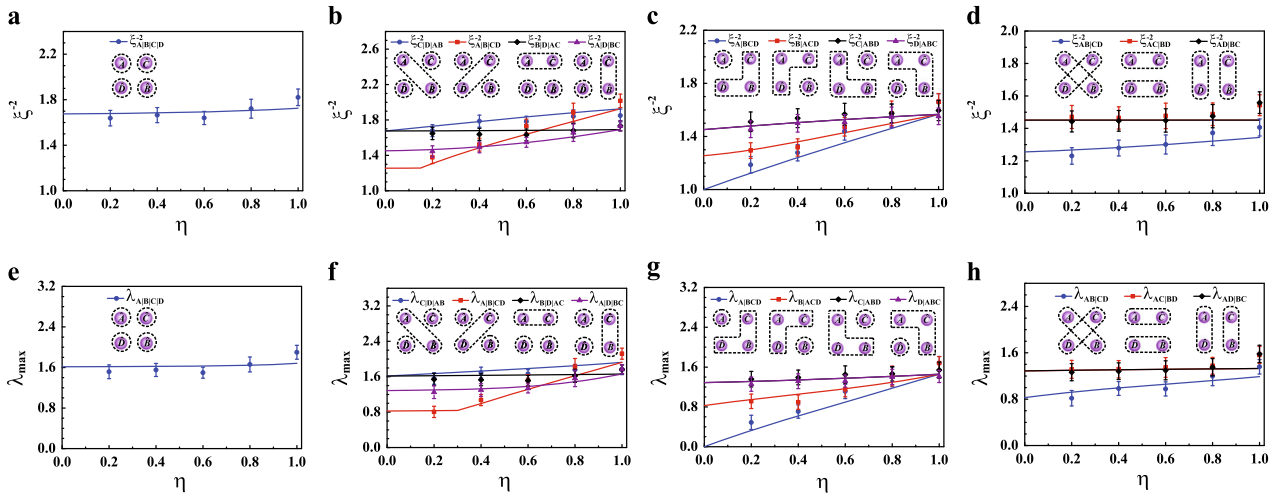

Fig. 4 Experimental results for the four-mode square Gaussian cluster state in a lossy channel with transmission efficiency η. **a**–**d** Inverse multi-mode squeezing coefficients ξ^{-2} for the partitions of classes 1⊗1⊗1⊗1, 1⊗1⊗2, 1⊗3, and 2⊗2, respectively. **e**–**h** The corresponding data for Gaussian Fisher information entanglement criterion. The data points are numerically optimized coefficients from experimentally obtained covariance matrices and the curves represent the corresponding numerically optimized predictions from the theoretical model

the quadrature $\hat{q}(\mathbf{g}) = (\hat{x}_B - \hat{x}_C)/\sqrt{2}$ is more pronounced as it does not decay with η, being independent of mode A. The discontinuity is therefore explained by a sudden change of the optimal squeezing direction due to depletion of mode A. We remark that the experimentally prepared states are the same, except for the variable η. The change of the squeezing direction simply implies that when the local noise exceeds a critical value, the entanglement is more easily revealed by analyzing the quantum state from a different "perspective" in phase space. Notice that having access to the full covariance matrix, we can analyze both entanglement witnesses for arbitrary directions.

The change of the optimal direction is observed for both entanglement coefficients, whereas the transition occurs at a larger value of η for the Fisher information criterion (4) (see Supplementary Information). There we also show the two-mode entanglement properties after tracing over one of the modes in an analysis of the reduced density matrices, which show that two-mode entanglement persists after tracing over one of the subsystems, in stark contrast to GHZ states of discrete variables.[34]

Finally, we analyze the four-mode square Gaussian cluster state in Fig. 4. We find that the decoherence of entanglement depends on the cluster state's geometric structure. As shown in Fig. 4a, the inverse multi-mode squeezing coefficient $\xi^{-2}_{A|B|C|D}$ for the fully separable partition is not sensitive to transmission loss on mode A, while decoherence affects the coefficients for other partitions shown in Fig. 4b–d. For 1⊗1⊗2 partitions, only the results of $\xi^{-2}_{C|D|AB}$, $\xi^{-2}_{A|B|CD}$, $\xi^{-2}_{B|D|AC}$, and $\xi^{-2}_{A|D|BC}$ are shown in Fig. 4b ($\xi^{-2}_{B|C|AD}$ and $\xi^{-2}_{A|C|BD}$ are shown in Fig. S3 in Supplementary Information). The discontinuity for the $A|B|CD$ partition is again explained by a transition of the optimal squeezing direction at a critical value of the transmission η for the isolated mode A (see Supplementary Information). The two coefficients $\xi^{-2}_{C|D|AB}$ and $\xi^{-2}_{A|B|CD}$ ($\xi^{-2}_{B|D|AC}$ and $\xi^{-2}_{A|D|BC}$) are equal for $\eta = 1$ because of the symmetric roles of these modes in these partitions. As shown in Fig. 4b, c, the most sensitive coefficients to transmission losses of mode A are those where mode A is an individual subsystem. The coefficients $\xi^{-2}_{C|ABD}$ and $\xi^{-2}_{D|ABC}$ overlap due to the symmetric roles of modes C and D.

Figure 4d shows the inverse multi-mode squeezing coefficients for 2⊗2 partitions. It is interesting that the coefficient $\xi^{-2}_{AC|BD}$ $\left(\xi^{-2}_{AD|BC}\right)$ is immune to transmission loss of mode A. This indicates that the collective coefficients for 2⊗2 partitions, where each partition is composed by two neighboring modes (recall the graph representation in Fig. 1c), are not sensitive to the loss of any one mode. In contrast, the coefficient $\xi^{-2}_{AB|CD}$, where each subsystem is composed by two diagonal modes, is still sensitive to transmission loss. As before, we find that the qualitative behavior of the

squeezing coefficient ξ^{-2} coincides with that of $\lambda_{\max}$ of the Gaussian Fisher information criterion (4), see Fig. 4e–h.

A further understanding of the entanglement structure is provided by an analysis of the three-mode and two-mode reduced density matrices of the state as well as of the optimal directions. A detailed analysis reveals that the loss-robustness is drastically reduced for all partitions if either mode C or D is traced out (see Supplementary Information). Moreover, for very small values of η, the entanglement in the partitions $A|CD$, $D|AB$, and $C|AB$ in the reduced three-mode states is revealed by the criterion (4) but not by the squeezing approximation (7), where we assumed $\mathbf{h} = \mathbf{\Omega g}$ to simplify the optimization (see Supplementary Information).

DISCUSSION

To benchmark our CV entanglement criteria, we may compare them to the PPT criterion, which is necessary and sufficient for $1\otimes(N-1)$ separability of Gaussian states.[9,10,35] For partitions into more than two subsystems the PPT criterion cannot be applied. It is interesting to notice that the PPT separability condition can be expressed as

$$\mathbf{\Gamma}_{\hat{\rho}^{\mathrm{PPT}}}^{-1} - 4\mathbf{\Omega}^T\mathbf{\Gamma}_{\hat{\rho}^{\mathrm{PPT}}}\mathbf{\Omega} \leq 0, \tag{8}$$

where $\Gamma_{\hat{\rho}^{\mathrm{PPT}}}$ is the covariance matrix after application of the partial transposition operation. The condition (8) is the Heisenberg–Robertson uncertainty relation for the state $\hat{\rho}^{\mathrm{PPT}}$ and constitutes a bona-fide condition for the physicality of the covariance matrix.[36] A violation of (8) therefore indicates that $\Gamma_{\hat{\rho}^{\mathrm{PPT}}}$ does not correspond to a physical state, from which one can conclude that the original state, described by $\Gamma_{\hat{\rho}^{\mathrm{PPT}}}$, is entangled. The similarity of Eqs. (4) and (8) indicates the close relationship of the two criteria with the uncertainty relation.[25] Note also that all pure Gaussian states Ψ saturate the uncertainty relation $\mathbf{\Gamma}_{\psi}^{-1} = 4\mathbf{\Omega}^T\mathbf{\Gamma}_{\psi}\mathbf{\Omega}$, which together with Eq. (1) allows us to recover the relation $F_Q[\Psi, \hat{q}(\mathbf{g})] = 4\mathbf{g}^T\mathbf{\Gamma}_{\psi}\mathbf{g}$ for pure states.

The criteria employed here and the well-established PPT condition are not equivalent. This is indicated by: (i) The applicability of our criteria to multi-partite separability classes, their geometric interpretation and their connection to metrological sensitivity. For example, we analyzed a total of 44 partitions for CV multi-mode entangled states of two, three, and four photonic modes. Out of these, 12 are genuine multi-partitions, which cannot be analyzed with the PPT criterion (see Supplementary Information for more details). (ii) The ability to detect non-Gaussian entanglement beyond the PPT condition using the CV Fisher information[18] or squeezing of higher-order observables.[25] (iii) The existence of PPT-entangled states which are not revealed by the CV squeezing coefficient or the Fisher information for displacements. A simple class of states that belong to (iii) can be constructed by mixing the two-mode Gaussian entangled state with the vacuum (see Supplementary Information). Moreover, the reduced two-mode states of the four-mode cluster state studied here also are examples of (iii).

In conclusion, we demonstrated that the multi-mode squeezing coefficient and the quantum Fisher information provide useful tools to understand the entanglement structure of Gaussian N-mode entangled states. In our microscopic analysis of CV states of up to four modes we characterized the robustness of entanglement for each partition individually. The effect of losses on more than one mode of three-mode and four-mode entangled states are also theoretically investigated, which confirms the resilience of multipartite CV Gaussian entanglement to finite losses (see Supplementary Information). The methods employed in this work yield a geometric interpretation in terms of a phase-space direction that identifies a strongly squeezed multi-mode quadrature as the origin of the mode correlations. Certain partitions revealed sudden transitions of the optimal phase-space direction for entanglement detection, rendering the entanglement coefficient invariant after passing a threshold value. This is strongly reminiscent of the "freezing" behavior previously observed for measures of entanglement,[37] discord,[38] and coherence[39] under incoherent dynamics. However, it is important to notice that the entanglement criteria considered here are witnesses of entanglement and do not represent quantitative measures in a strict sense.

The squeezing coefficient represents an easily accessible entanglement criterion, based on a second-order approximation of the quantum Fisher information, which is more involved to extract experimentally for general states. For the specific case of Gaussian states, both criteria are expressed in terms of moments up to second order, but for the squeezing coefficient the optimization was restricted to specific quadratures to reduce the number of parameters. This was found to be a suitable approximation in most cases, as we obtained qualitatively equivalent results to the Fisher information. Only in the presence of strong losses, the Fisher information reveals Gaussian entanglement for certain partitions of the reduced states that remains undisclosed by the squeezing coefficient.

Our detailed analysis highlights the advantages of the mode entanglement criteria based on the quantum Fisher information for Gaussian states, in particular, their ability to study multi-partitions based on available data only, their geometric interpretation, and their relation to the metrological sensitivity. We have also observed their limitations, i.e., not being a necessary and sufficient condition for all Gaussian states. However, in principle the entanglement of arbitrary pure states can be revealed using the Fisher information criterion.[18] These methods thus complement the well-established PPT techniques for CV systems, which are necessary and sufficient for Gaussian $1\otimes(N-1)$ systems but unfitting for multi-partitions and of limited applicability for non-Gaussian states.

The more general criterion based on the quantum Fisher information is expected to be particularly useful for non-Gaussian states. In this case, it is able to reveal entanglement even when entanglement criteria based on second-order moments can no longer be applied and the concept of squeezing is ill-defined. We expect that these methods provide useful techniques for the analysis of entanglement in complex CV networks.[26]

METHODS

Details of experiment

The experimental setup to generate the CV two-mode Gaussian entangled state is depicted in Fig. 1f. A −3 dB two-mode Gaussian entangled state at the sideband frequency of 3 MHz is generated directly from a NOPA I. The LC is composed by a HWP and a PBS. Quadratures are measured via homodyne detectors $(\mathrm{HD})_{1-2}$ and the local oscillator (LO).

The three-mode GHZ state is generated using the experimental setup depicted in Fig. 1g. The squeezed states are generated from the coupled modes at +45° and −45° polarization directions of two NOPAs. Further technical details can be found in ref. [30]

Figure 1h depicts the experimental setup used to generate the four-mode Gaussian square cluster state. A dual-wavelength laser for 540 and 1080 nm is used. Two mode cleaners are inserted between the laser source and the NOPAs to filter higher-order spatial modes and noise of the laser beams at two wavelengths, respectively. In addition to elements described already for Fig. 1f, g, dichroic mirrors (DMs) are also shown. For technical details we refer to ref. [31]

Reconstruction of covariance matrices

In the experiment, the covariance matrices of the multipartite CV entangled states are obtained from local measurements on the optical output modes. These measurements include the amplitude and phase quadratures $\Delta^2\hat{r}_i$, $\Delta^2\hat{r}_j$, and the cross-correlations $\Delta^2(\hat{r}_i + \hat{r}_j)$ or $\Delta^2(\hat{r}_i - \hat{r}_j)$.

The elements of the covariance matrix are calculated via the identity

$$(\mathbf{\Gamma}_{\hat{\rho}})_{ij} = \frac{1}{2}\left[\Delta^2(\hat{r}_i + \hat{r}_j) - \Delta^2\hat{r}_i - \Delta^2\hat{r}_j\right],$$
$$(\mathbf{\Gamma}_{\hat{\rho}})_{ij} = -\frac{1}{2}\left[\Delta^2(\hat{r}_i - \hat{r}_j) - \Delta^2\hat{r}_i - \Delta^2\hat{r}_j\right]. \quad (9)$$

For each transmission efficiency η of mode A, three sets of covariance matrices are reconstructed. Error bars for all the experimental data are obtained from the statistics of the three covariance matrices.

DATA AVAILABILITY

The data that support the findings of this study are available from the corresponding author on request.

ACKNOWLEDGEMENTS

This research was supported by the National Natural Science Foundation of China (Grant Nos. 11522433, 11834010, 61601270, 61475092, and 11874247), National Key R&D Program of China (Grant Nos. 2016YFA0301402, 2017YFA0304500, and 2017YFA0304203), 111 project (Grant No. D18001), the Hundred Talent Program of the Shanxi Province (2018), Fund for Shanxi "1331" Project Key Subjects Construction, and the European Commission through the Quant-ERA project "CEBBEC". X.S. thanks the program of Youth Sanjin Scholar. M.G. thanks the Alexander von Humboldt foundation for support. W.L. thanks PCSIRT (Grant No. IRT_17R70), and the Program of State Key Laboratory of Quantum Optics and Quantum Optics Devices (No. KF201703).

AUTHOR CONTRIBUTIONS

M.G., W.L., X.S., and A.S. conceived the idea. X.S. and K.P. designed the experiment. Z. Q., X.D., and X.S. constructed and performed the experiment. D.H. participated in part of the experiment. Z.Q., Z.R., and M.G. analyzed the data. M.G. and Z.Q. wrote the manuscript with input from Z.R., W.L., X.S., and A.S. All authors participated in the discussion of the results and commented on the manuscript.

ADDITIONAL INFORMATION

Supplementary information accompanies the paper on the *npj Quantum Information* website (https://doi.org/10.1038/s41534-018-0119-6).

Competing interests: The authors declare no competing interests.

Publisher's note: Springer Nature remains neutral with regard to jurisdictional claims in published maps and institutional affiliations.

REFERENCES

1. Nielsen, M. A. & Chuang, I. L. *Quantum Computation and Quantum Information*. (Cambridge University Press, New York, NY, 2000).
2. Braunstein, S. L. & van Loock, P. Quantum information with continuous variables. *Rev. Mod. Phys.* **77**, 513 (2005).
3. Weedbrook, C. et al. Gaussian quantum information. *Rev. Mod. Phys.* **84**, 621–669 (2012).
4. Walther, P. et al. Experimental one-way quantum computing. *Nature* **434**, 169–176 (2005).
5. Ukai, R. et al. Demonstration of unconditional one-way quantum computations for continuous variables. *Phys. Rev. Lett.* **106**, 240504 (2011).
6. Su, X. et al. Gate sequence for continuous variable one-way quantum computation. *Nat. Commun.* **4**, 2828 (2013).
7. Giovannetti, V., Lloyd, S. & Maccone, L. Advances in quantum metrology. *Nat. Photonics* **5**, 222 (2011).
8. Lu, H. et al. EntanglementStructure: entanglement partitioning in multipartite systems and its experimental detection using optimizable witnesses. *Phys. Rev. X* **8**, 021072 (2018).
9. Duan, L.-M., Giedke, G., Cirac, J. I. & Zoller, P. Inseparability criterion for continuous variable systems. *Phys. Rev. Lett.* **84**, 2722 (2000).
10. Simon, R. Peres–Horodecki separability criterion for continuous variable systems. *Phys. Rev. Lett.* **84**, 2726 (2000).
11. Gühne, O. & Tóth, G. Entanglement detection. *Phys. Rep.* **474**, 1 (2009).
12. van Loock, P. & Furusawa, A. Detecting genuine multipartite continuous-variable entanglement. *Phys. Rev. A* **67**, 052315 (2003).
13. Sperling, J. & Vogel, W. Multipartite entanglement witnesses. *Phys. Rev. Lett.* **111**, 110503 (2013).
14. Gerke, S. et al. Full multipartite entanglement of frequency-comb Gaussian states. *Phys. Rev. Lett.* **114**, 050501 (2015).
15. Chen, M., Menicucci, N. C. & Pfister, O. Experimental realization of multipartite entanglement of 60 modes of a quantum optical frequency comb. *Phys. Rev. Lett.* **112**, 120505 (2013).
16. Su, X. et al. Experimental preparation of quadripartite cluster and Greenberger–Horne–Zeilinger entangled states for continuous variables. *Phys. Rev. Lett.* **98**, 070502 (2007).
17. Yokoyama, S. et al. Ultra-large-scale continuous-variable cluster states multiplexed in the time domain. *Nat. Photonics* **7**, 982–986 (2013).
18. Gessner, M., Pezzè, L. & Smerzi, A. Efficient entanglement criteria for discrete, continuous, and hybrid variables. *Phys. Rev. A* **94**, 020101(R) (2016).
19. Pezzè, L., Smerzi, A., Oberthaler, M. K., Schmied, R. & Treutlein, P. Non-classical states of atomic ensembles: fundamentals and applications in quantum metrology. *Rev. Mod. Phys.* **90**, 035005 (2018).
20. Wineland, D. J., Bollinger, J. J., Itano, W. M., Moore, F. L. & Heinzen, D. J. Spin squeezing and reduced quantum noise in spectroscopy. *Phys. Rev. A* **46**, R6797(R) (1992).
21. Sørensen, A., Duan, L.-M., Cirac, J. I. & Zoller, P. Many-particle entanglement with Bose–Einstein condensates. *Nature* **409**, 63 (2001).
22. Lücke, B. et al. Twin matter waves for interferometry beyond the classical limit. *Science* **334**, 773 (2011).
23. Strobel, H. et al. Fisher information and entanglement of non-Gaussian spin states. *Science* **345**, 424 (2014).
24. Bohnet, J. G. et al. Quantum spin dynamics and entanglement generation with hundreds of trapped ions. *Science* **352**, 1297 (2016).
25. Gessner, M., Pezzè, L. & Smerzi, A. Entanglement and squeezing in continuous-variable systems. *Quantum* **1**, 17 (2017).
26. Armstrong, S. et al. Programmable multimode quantum networks. *Nat. Commun.* **3**, 1026 (2012).
27. Braunstein, S. L. & Caves, C. M. Statistical distance and the geometry of quantum states. *Phys. Rev. Lett.* **72**, 3439 (1994).
28. Pinel, O., Jian, P., Treps, N., Fabre, C. & Braun, D. Quantum parameter estimation using general single-mode Gaussian states. *Phys. Rev. A* **88**, 040102(R) (2013).
29. Jiang, Z. Quantum Fisher information for states in exponential form. *Phys. Rev. A* **89**, 032128 (2014).
30. Deng, X., Tian, C., Su, X. & Xie, C. Avoiding disentanglement of multipartite entangled optical beams with a correlated noisy channel. *Sci. Rep.* **7**, 44475 (2017).
31. Deng, X. et al. Demonstration of monogamy relations for Einstein–Podolsky–Rosen steering in Gaussian cluster states. *Phys. Rev. Lett.* **118**, 230501 (2017).
32. Barbosa, F. A. S. et al. Robustness of bipartite Gaussian entangled beams propagating in lossy channels. *Nat. Photonics* **4**, 858–861 (2010).
33. Adesso, G., Serafini, A. & Illuminati, F. Multipartite entanglement in three-mode Gaussian states of continuous-variable systems: quantification, sharing structure, and decoherence. *Phys. Rev. A* **73**, 032345 (2006).
34. Dür, W., Vidal, G. & Cirac, J. I. Three qubits can be entangled in two inequivalent ways. *Phys. Rev. A* **62**, 062314 (2000).
35. Werner, R. F. & Wolf, M. M. Bound entangled Gaussian states. *Phys. Rev. Lett.* **86**, 3658 (2001).
36. Simon, R., Mukunda, N. & Dutta, B. Quantum-noise matrix for multimode systems: U(n) invariance, squeezing, and normal forms. *Phys. Rev. A* **49**, 1567 (1994).
37. Carnio, E. G., Buchleitner, A. & Gessner, M. Robust asymptotic entanglement under multipartite collective dephasing. *Phys. Rev. Lett.* **115**, 010404 (2015).
38. Haikka, P., Johnson, T. H. & Maniscalco, S. Non-Markovianity of local dephasing channels and time-invariant discord. *Phys. Rev. A* **87**, 010103(R) (2013).
39. Bromley, T. R., Cianciaruso, M. & Adesso, G. Frozen quantum coherence. *Phys. Rev. Lett.* **114**, 210401 (2015).